Biosensors and Bioelectronics 132 (2019) 62–67

Contents lists available at ScienceDirect

Biosensors and Bioelectronics

journal homepage: www.elsevier.com/locate/bios

Highly-efficient luminol immobilization approach and exponential strand displacement reaction based electrochemiluminescent strategy for monitoring microRNA expression in cell

Yali Yuan[1], Xue Li[1], An-Yi Chen, Hai-Jun Wang, Ya-Qin Chai*, Ruo Yuan*

Key Laboratory of Luminescent and Real-Time Analytical Chemistry (Southwest University), Ministry of Education, College of Chemistry and Chemical Engineering, Southwest University, Chongqing 400715, China

ARTICLE INFO

Keywords:
Electrochemiluminescence
Cruciform DNA structure
Exponential strand displacement reaction
π-π stacking interaction

ABSTRACT

This work used 3,4,9,10-perylenetetracarboxylic acid-luminol composite (PTCA-luminol) as signal tag with improved ECL signal and applied cruciform DNA structure mediated exponential strand displacement reaction (SDR) to construct an ultrasensitive electrochemiluminescence (ECL) biosensor for microRNA-21 (miRNA-21) detection. The novel luminol-based signal tags was synthesized utilizing the π-π stacking interaction between PTCA and luminol, realizing highly effective and stable immobilization of luminol and resulting in good stability and strong ECL response. Meanwhile, target miRNA-21 triggered disaggregation of cruciform DNA structure was used to mediate exponential SDR for target recycling amplification. Taking advantage of the novel luminol-based signal tag and exponential SDR, the proposed ECL biosensor achieved excellent sensitivity with wide linear range from 10 aM to 100 pM and detection limit was 2 aM. Moreover, this ECL biosensor was applied to estimate the expression level of miRNA-21 and pharmacodynamics of matrine in human breast cancer cells (MCF-7 cells). The proposed biosensor provided a new opportunity for the preparation of ECL nanomaterials and exhibited great application potential in other biomarkers detection, clinical application and pharmacodynamics evaluation.

1. Introduction

Luminol is one of the most widely used electrochemiluminescence (ECL) luminophore in sensitive determination of various kinds of biomarkers including proteins, DNAs, microRNAs (miRNAs), cells and so on due to its low cost and toxic, and high light-emitting quantum yield (Huo et al., 2018; Xu et al., 2016; Khonsari and Sun, 2017; Kitte et al., 2017; Miao, 2008; Wu et al., 2017; Zhang et al., 2018). In universal research works, luminol was directly added into detection solution to achieve stable ECL signal due to its advantages of good stability and simple operation. (Zhao et al., 2017, 2015; Zhang et al., 2015) However, the detection relied on the ECL enhancing or quenching of the original ECL signal, which led to relatively high noise and went against the improvement of sensitivity. To improve the sensitivity, coreaction accelerator strategy and high-efficient immobilization strategy for luminorphor are the core of research. In recent years, researchers devoted themselves to develop luminol-based signal tag obtained by immobilizing luminol *via* physical adsorptions and crosslinking reactions to decrease the noise and improve sensitivity. Cui's group used luminol to reduce chloroauric acid directly and produced luminol-capped gold nanoparticles (Cui et al., 2007; Chen et al., 2014; Gu et al., 2015; Zhou et al., 2017; Wang et al., 2016a, 2016b). This method afforded an easy-but-reliable approach for the immobilization of luminol, while the operation was relatively complicated. In our previous works, we achieved luminol immobilization *via* the crosslinking amino group of luminol and carboxyl groups of other nanomaterials with a relatively simple operation (Wang et al., 2016a, 2016b; Liu et al., 2017a, 2017b). Nevertheless, the immobilization quantity was restricted by the relatively low crosslinking activity of amine group on the benzene ring. Thus, it is important but still a challenge to develop an effective method for luminol immobilization. Notably, the π-π stacking interaction is an efficient and stable method to prepare nanomaterials containing delocalized structure, such as graphene, hemin and 3,4,9,10-perylenetetracarboxylic acid (PTCA) (Lee et al., 2011; Shen et al., 2012; Xue et al., 2012). Herein, a novel luminol-based ECL signal tag was prepared by π-π stacking interaction between luminol and PTCA for efficiently immobilizing luminol.

Enzyme-free amplification strategies, such as hybridization chain

* Corresponding authors.
E-mail addresses: yqchai@swu.edu.cn (Y.-Q. Chai), yuanruo@swu.edu.cn (R. Yuan).
[1] The first two authors have equal contribution to the work.

https://doi.org/10.1016/j.bios.2019.02.005
Received 5 December 2018; Received in revised form 8 January 2019; Accepted 3 February 2019
Available online 23 February 2019
0956-5663/

reaction (HCR) (Yin et al., 2016; Tang et al., 2017; Liu et al., 2017a, 2017b), catalyst hairpin assembly (CHA), (Jiang et al., 2013; Li et al., 2016) and strand displacement reaction (SDR) (Wang et al., 2017; Zhang et al., 2016) with the advantages of easy operation, broad practicability and low cost, show promising potentials for biosensing, for example Liao and coworkers used hybridization chain reaction (HCR) to construct AT-rich dsDNA for the immobilization of luminophore Cu NCs, achieving high luminescence intensity with the help of coreaction accelerator. (Liao et al., 2018) Unfortunately, the sensitivity of common enzyme-free amplification strategies was limited due to their linear target recycling amplification from target to outputs. Therefore, it is of great significance to develop a more efficient target recycling amplification strategy to improve the sensitivity of bioanalysis. In this work, based on a novel cruciform DNA structure, an exponential SDR was firstly put forward to achieve more sensitive target recycling amplification. With the introduction of target, the cruciform DNA structure was disaggregated, accompanying with target and target mimics released, which both could participate in next cycle to realize exponential target recycling amplification.

Herein, an ultrasensitive ECL biosensor was proposed for determination of miRNA-21 based on high-performance luminol-based signal tag and cruciform DNA structure mediated exponential SDR. The signal tag (Scheme 1A) achieved stable and efficient immobilization of luminol, which provided a novel avenue for preparing high-performance luminol-based ECL signal tag. Moreover, the novel cruciform DNA structure mediated exponential SDR was designed for exponential target recycling amplification to further improve the sensitivity. As shown in Scheme 1B, the cruciform DNA structure consisted by D1, thiol-modified D2, D3 (target mimics) and D4. In the presence of target miRNA-21, signal tag labeled H1 could be unfolded to expose 3′-terminus of H1 for hybridization with D2 to release miRNA-21, D1, D3 and D4. With D1 and D4 discarded, D3 and released miRNA-21 could unfold another signal tag labeled H1 for next cycle, achieving exponential target recycling amplification. As a result, the luminol-based signal tag was fabricated on the electrode as H1 hybridized with D2, producing strong ECL response. With the combination of luminol-based signal tag and cruciform DNA structure mediated exponential SDR, the proposed biosensor achieved good performance for detection of miRNA-21 with a low detection limit of 2 aM. Impressively, the proposed biosensor showed good response to human breast cancer cell lines (MCF-7 cells) with the cell numbers increased. What's more, when the MCF-7 cells were treated by different concentration of matrine, the ECL responses decreased with the increase of matrine concentration indicating that matrine is available to inhibit the expression of miRNA-21 in MCF-7 cells. This method presents a new chance to prepare high-performance ECL signal tag, which also showed great promising for other miRNAs

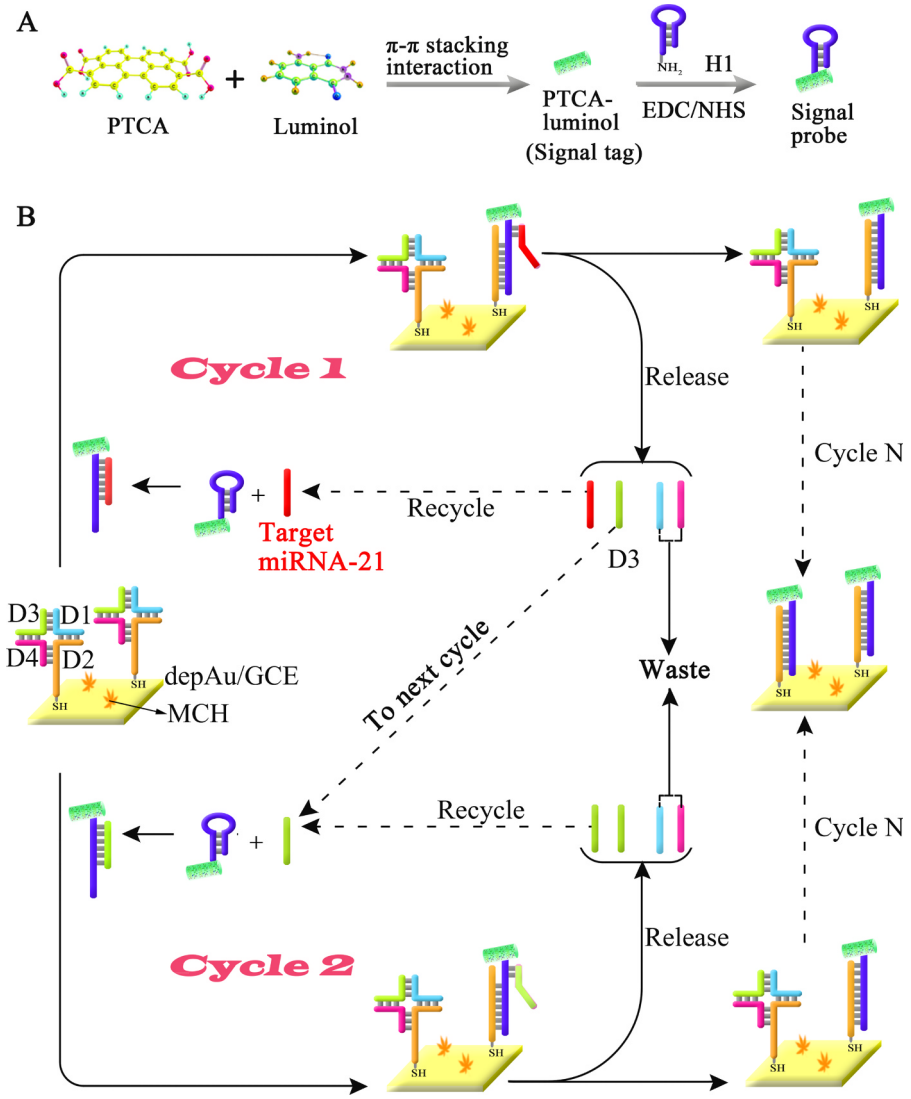

Scheme 1. (A) The preparation of luminol-based signal tag and signal probe; (B) The fabrication of the ECL biosensor and cruciform DNA structure mediated exponential SDR.

detection, pharmacodynamic evaluation and clinical diagnosis.

2. Experimental sections

2.1. Preparation of PTCA-luminol (signal tag) and H1-PTCA-luminol (signal probe)

At first, PTCDA was hydrolyzed by NaOH (1.0 M). And then, the pH of the solution was regulated to 6. After centrifugation, the PTCA was obtained (Huang et al., 2018). Then, the prepared PTCA aqueous solution was added into 2 mL luminol (0.05 M in 0.01 M NaOH) to stir for 24 h at 4 °C. To obtain signal tag, these precipitate were centrifuged and washed at 12,000 rpm for six times. After that, the carboxyl groups of signal tag were activated by EDC/NHS mixture solution at a 5:1 M stoichiometry for 2 h. Finally, 5′-amino-modified H1 was added into the above solution to reach a final concentration 1 μM at 4 °C for 12 h with continuous stirring. Thus, the signal probe was obtained and kept at 4 °C for further use.

2.2. Fabrication of the ECL biosensor

The mixed DNAs containing 2 μM D1, 2 μM D2, 2 μM D3 and 2 μM D4 in TE buffer were annealed at 95 °C for 5 min followed by gradient cooling to 8 °C to form the cruciform DNA structure for further use. Meanwhile, the glassy carbon electrode (GCE) was carefully polished according to the literature before modification (Xu et al., 2018). After drying, the GCE was immersed into $HAuCl_4$ (*w/v*, 1%) and electro-deposited AuNPs at −0.2 V for 30 s. Next, 10 μL cruciform DNA structure (see Supporting information) was incubated on the modified GCE for 15 h at 4 °C. Then, MCH (1 mM, 10 μL) was incubated 30 min to block the nonspecific binding sites.

2.3. Measurements of the ECL biosensor

Before measurement, 10 μL miRNA-21 and 10 μL signal probe were incubated on the prepared electrode at 37 °C for 90 min. Then, the modified electrode was put into phosphate-buffered solution (pH = 7.4) (containing 10 μM H_2O_2), and the ECL signals were recorded by MPI-E ECL analyzer scanning from 0.2 V to 0.8 V with scanning rate of 100 mV/s.

3. Results and discussion

3.1. Characteristics of PTCA and PTCA-luminol

SEM was employed to reveal surface morphology of PTCA and PTCA-luminol. As shown in Fig. 1A, the SEM image showed that PTCA was uniform cylindrical-like morphology, which was conformed to the literature indicating the successful preparation of PTCA (Cang et al., 2015). Compared with the pure PTCA cylindrical-like particles, the morphology of PTCA-luminol (Fig. 1B) showed irregular, smaller and spiculate cylindrical-like, indicating the successful preparation of the PTCA-luminol.

Furthermore, the detailed elemental analysis of PTCA-luminol composite was performed by XPS. The characteristic peaks at 285.08, 400.08 and 531.68 eV in the full region of PTCA-luminol (Fig. 1C) could be attributed to C1s, N1s, O1s, respectively, where the N 1s core levels only derived from luminol and the O1s core levels indicated the presence of PTCA. The enlarged curve of C1s, N1s, O1s regions displayed in Fig. 1D. The result demonstrated that both PTCA and luminol were involved in the composites.

FTIR spectra were recorded to investigate the interaction between PTCA and luminol. In Fig. 1E, the 1772.71 cm^{-1} peak (the vibration of C = O) was belong to carboxyl groups of PTCA (curve a). Luminol showed absorption peak at 3455.97 cm^{-1} on behalf of the characteristic of N-H bond combined with benzene structure (curve b). In PTCA-luminol composite (curve c), the characteristic peaks of carboxyl group and N-H bond still existed. Compared with individual luminol and PTCA, the characteristic peaks of carboxyl group and N-H bond in PTCA-luminol composite shifted to 3423.47 cm^{-1} and 1760.57 cm^{-1} respectively, indicating that the reaction between PTCA and luminol was noncovalent reaction.

Furthermore, UV–vis absorption spectra were applied to further study the interaction between PTCA and luminol. In Fig. 1F, PTCA in aqueous solution displayed an optical absorption spectrum of 459 nm because of perylene core π-π* transition (curve a). Two peaks of luminol at 293 nm and 350 nm were observed (curve b). For PTCA-luminol, there displayed three peaks at 292 nm, 350 nm and 465 nm (curve c), intimating electron interaction in PTCA-luminol occurred. After luminol was adsorbed on PTCA successfully, the electron interaction in PTCA-luminol might promote π-electron delocalization of aromatic ring, leading to lower π-π* energy gap of PTCA and red-shift peak, indicating that it was π-π stacking interaction in PTCA-luminol composite.

3.2. Investigation of ECL mechanism of PTCA-luminol

To demonstrate the luminescence mechanism of PTCA-luminol composite, fluorescence emission spectra and ECL emission spectrum were obtained. As exhibited in Fig. 2A, the fluorescence emission spectra of luminol (curve a) was single characteristic maximum emission peak on 426 nm when the excitation wavelength was 350 nm. And the PTCA-luminol (curve b) was also single characteristic maximum emission peak at 425.4 nm during the same excitation wavelength, indicating that luminol was the only luminophore in the composite. Simultaneously, the normalized ECL spectrum was measured by alternately alter the optical filters. For the ECL emission spectrum of PTCA-luminol (Fig. 2B), the ECL emission peak was situated at 425 nm, matching with the emission peak of traditional luminol/H_2O_2 ECL system in previous literature. (Dong et al., 2014) Based on the previous results, a schematic illustration for the probable ECL mechanism of PTCA-luminol composite could be expounded as displayed in Scheme 2. That showed main reactions including (1) the decomposition of H_2O_2 to produce $O_2^{-\bullet}$; (2) the conversion of PTCA-luminol into PTCA-luminol$^-$; (3) the oxidation of PTCA-luminol$^-$ to PTCA-luminol$^{-\bullet}$; (4) the oxidation of PTCA-luminol$^{-\bullet}$ to 3-aminophthalate (AP^{2-*}); (5) the production of emit light when AP^{2-*} was transformed to AP^{2-}. The reaction equations are as follows (LH stands for luminol):

$$\mathbf{H_2O_2 \rightarrow H^+ + HOO^- \rightarrow OH^- + \bullet O_2H \rightarrow O_2^{\bullet -} + H^-} \quad (1)$$

$$\mathbf{PTCA - LH^- - e \rightarrow PTCA - LH^{\bullet} \rightarrow PTCA - L^- + H^+} \quad (2)$$

$$\mathbf{PTCA - L^- + O_2^- \rightarrow PTCA - LO_2^{2-}} \quad (3)$$

$$\mathbf{PTCA - LO_2^{2-} \rightarrow PTCA - AP^{2-*} + N_2} \quad (4)$$

$$\mathbf{PTCA - AP^{2-*} \rightarrow PTCA - AP^{2-} + \boldsymbol{h\nu}} \quad (5)$$

3.3. Detection performance of the biosensor

To estimate biosensors' performance, the ECL signals with different concentration of miRNA-21 were measured in the optimized condition (Fig. S-3 listed in Supporting information). As displayed in Fig. 3A, a gradual increase of ECL intensity occurred with increasing miRNA-21 concentration. A good linear range from 10 aM to 100 pM with the detection limit down to 2 aM (S/N = 3) was obtained in Fig. 3B. And the linear equation was $I = 21{,}956.4 + 1079.8 \lg c$ (where I stands for the ECL intensity, c strands for miRNA-21 concentration) with a correlation coefficient of 0.9943, which was more sensitive than other previously reported method for miRNA-21 detection (Table 1). The reason can be ascribed as follows: first, the luminol based high-performance ECL signal tag achieved nondestructive and efficient

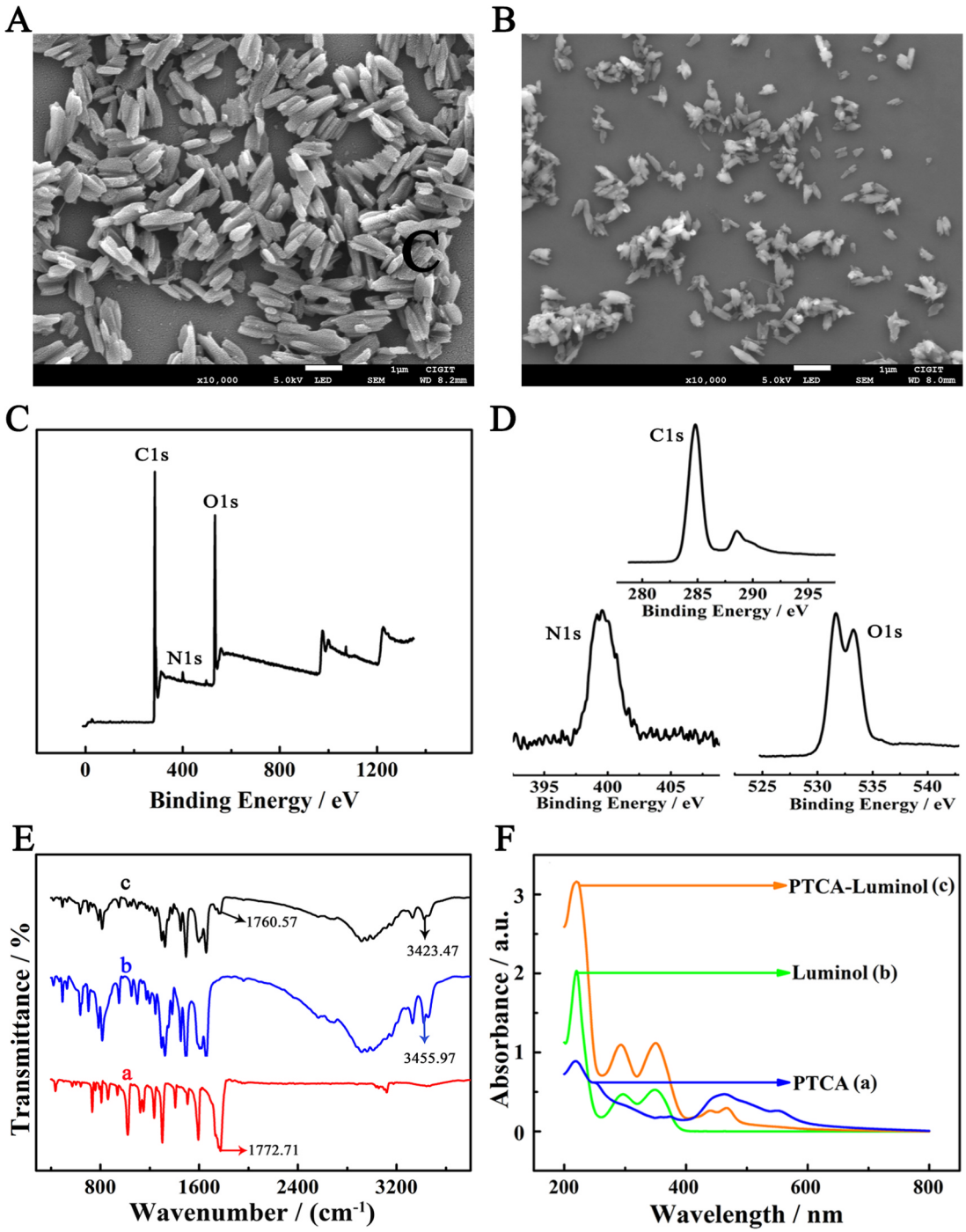

Fig. 1. The SEM characterization for PTCA (A) and PTCA-luminol (B); the XPS analysis for PTCA-luminol (C) and enlarged curves of C1s, N1s and O1s (D), and the FTIR spectra (E) and UV–vis absorption spectra (F) characterization of PTCA (a), luminol (b) and PTCA-luminol (c).

immobilization of luminol. Moreover, the cruciform DNA structure mediated exponential SDR presented high amplification efficiency with significantly improved sensitivity of the biosensor.

3.4. Application of the biosensor for miRNA-21 monitor

To test feasibility of this biosensor in tumor cells, a series of determination experiments was constructed in different cell numbers of MCF-7 cell lines and Hela cell lines, respectively. Besides, MCF-7 cell lines were treated with different concentrations of matrine (0 μL/mL, 20 μL/mL, 40 μL/mL and 60 μL/mL) to evaluate pharmacodynamics of matrine. As displayed in Fig. 4A, the experiments were completed by ten times increasing MCF-7 and Hela cell numbers from 10 to 10,000 cells without matrine. It could be found that the ECL intensity both increased accordingly to the MCF-7 and Hela cell numbers from 10 to 10,000 cells without matrine, which matched with the previous literatures (Si et al., 2007; Ye et al., 2017), indicating that the proposed ECL biosensor could be used for quantitative miRNA-21 detection. What's more, as shown in Fig. 4B, the higher matrine concentration decreased ECL signals indicating the decreased quantity of miRNA-21. That demonstrated matrine could inhibit the expression of miRNA-21 in MCF-7 cells. (Li et al., 2012)

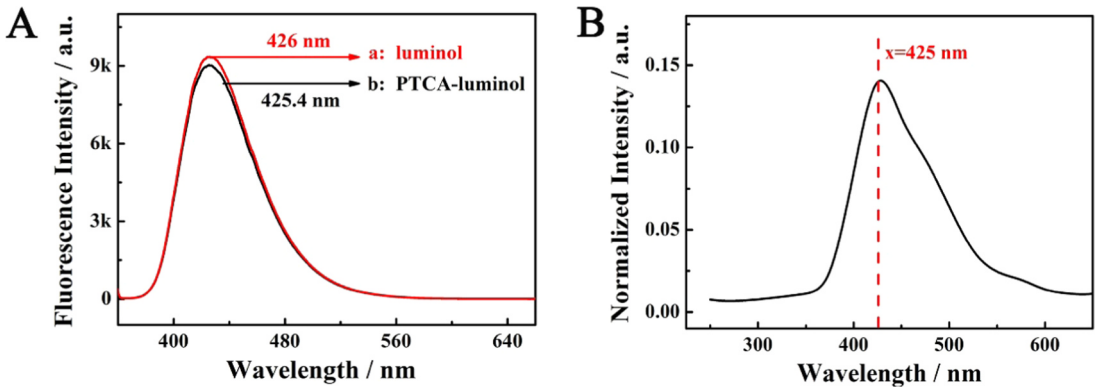

Fig. 2. (A) The fluorescence emission spectra of luminol (a) and PTCA-luminol (b). (B) The normalized ECL emission spectrum of PTCA-luminol.

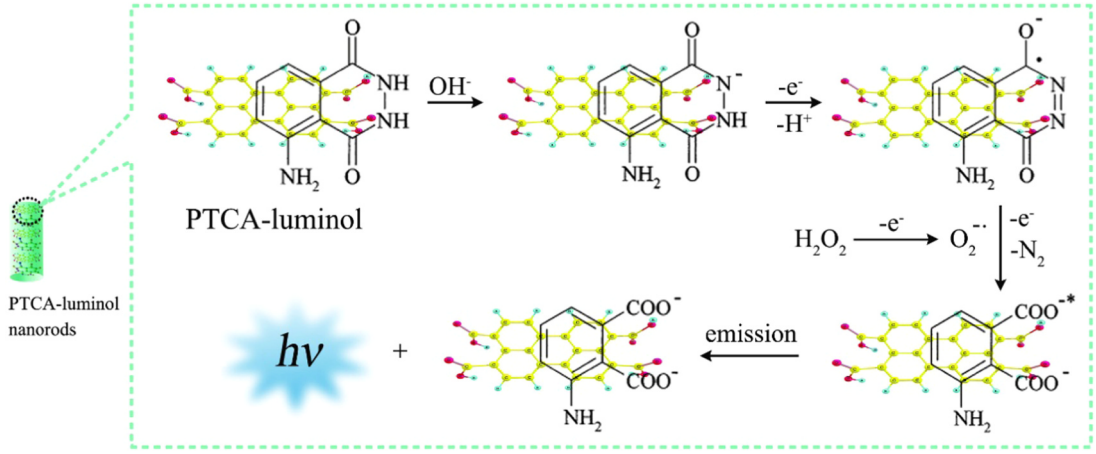

Scheme 2. Schematic ECL mechanism of PTCA-luminol composite.

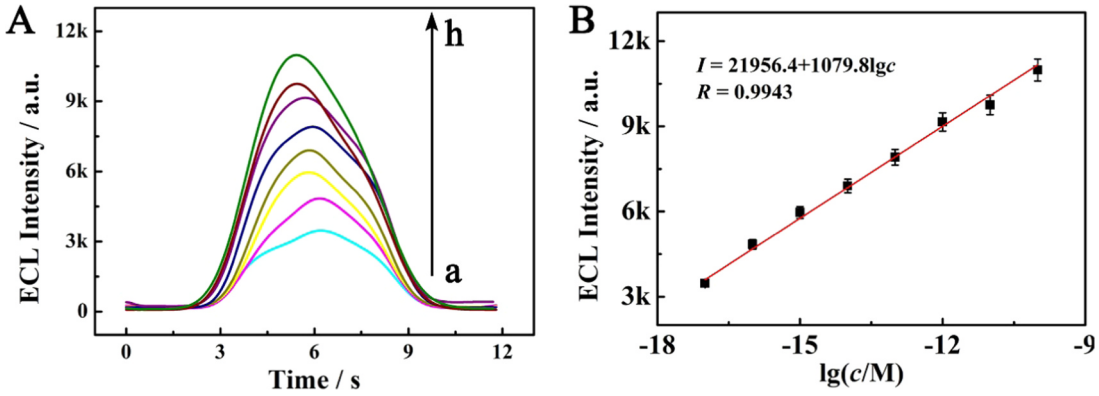

Fig. 3. (A) ECL signals in the presence of different concentration of miRNA-21 from a to h: (a) 10 aM, (b) 100 aM, (c) 1 fM, (d) 10 fM, (e) 100 fM, (f) 1 pM, (g) 10 pM and (h) 100 pM (B) The calibration plot of ECL intensities vs the logarithm of miRNA-21 concentration. Error bars: standard deviation (SD), $n = 4$.

Table 1
Comparison of Different Methods for MicroRNA-21 Detection.

Detection method	Linear range	Detection limit	Ref.
DPV	100 aM to 1 nM	78 aM	(Tian et al., 2018)
FL	1 fM to 50 pM	0.27 fM	(Yin et al., 2017)
SERS	100 aM to 100 pM	70.2 aM	(He et al., 2017)
ECL	1 fM to 1 nM	33 aM	(Feng et al., 2016)
ECL	10 aM to 100 pM	2 aM	This work

4. Conclusions

In summary, we constructed an ultrasensitive ECL biosensor for miRNA-21 determination with the combination of high-performance luminol-based signal tag and cruciform DNA structure mediated exponential SDR. This method opened up new trails for the immobilization of luminol and showed great potential for other high-performance ECL signal tag preparation. Besides, the cruciform DNA structure mediated exponential SDR presented high amplification efficiency and improved the sensitivity of the biosensor, holding great promise for applications in sensitive biomarker detection for clinical diagnostics.

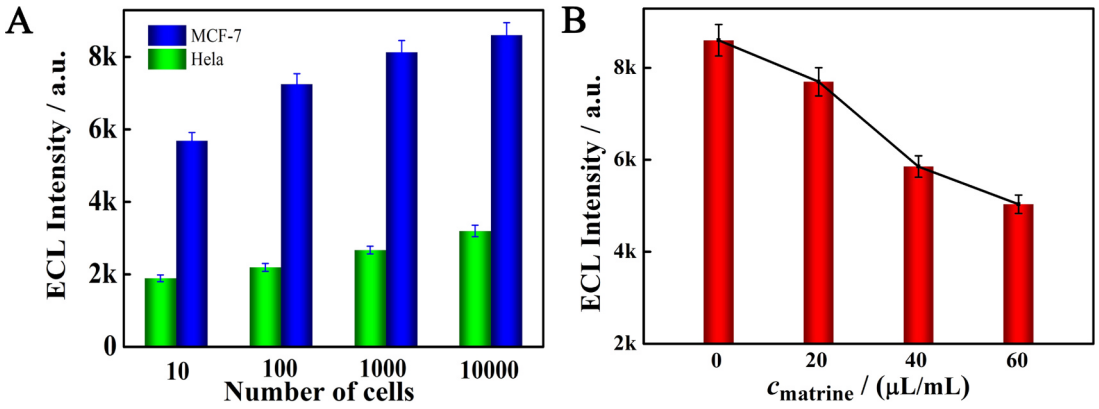

Fig. 4. ECL responses for the fabricated biosensor incubated with the RNA solutions extracted from (A) MCF-7 cells with different numbers (10, 100, 1000, 10,000 cells) and (B) 10,000 MCF-7 cells treated with different matrine concentrations (0, 20, 40, 60 μL/mL). Error bars: standard deviation (SD), $n = 4$.

Acknowledgement

This work was financially supported by the National Natural Science Foundation of China (NNSF) (21675129, 21775124, 21505107 and 51473136), the Chongqing Research Program of Basic Research and Frontier Technology (cstc2018jcyjA0797).

Declaration of interests

None.

Credit author statement

All authors have given approval to the final version of the manuscript.

Appendix A. Supplementary material

Supplementary data associated with this article can be found in the online version at doi:10.1016/j.bios.2019.02.005.

References

Cang, Y.Y., Xie, S.B., Chai, Y.Q., Yuan, Y.L., Yuan, R., 2015. Chem. Commun. 51, 7657–7660.
Chen, Y., Huang, Y., Lei, J.P., Zhang, L., Ju, H.X., 2014. Anal. Chem. 86, 5158–5163.
Cui, H., Wang, W., Duan, C.F., Dong, Y.P., Guo, J.Z., 2007. Chem. Eur. J. 13, 6975–6984.
Dong, Y.P., Gao, T.T., Zhou, Y., Zhu, J.J., 2014. Anal. Chem. 86, 11373–11379.
Feng, Q.M., Shen, Y.Z., Li, M.X., Zhang, Z.L., Zhao, W., Xu, J.J., Chen, H.Y., 2016. Anal. Chem. 88, 937–944.
Gu, W.L., Deng, X., Gu, X.X., Jia, X.F., Lou, B.H., Zhang, X.W., Li, J., Wang, E.K., 2015. Anal. Chem. 87, 1876–1881.
He, Y., Yang, X., Yuan, R., Chai, Y.Q., 2017. Anal. Chem. 89, 2866–2872.
Huang, L.J., Zhang, L., Yang, L., Yuan, R., Yuan, Y.L., 2018. Bionsens. Bioelectron. 104, 21–26.
Huo, X.L., Zhang, N., Yang, H., Xu, J.J., Chen, H.Y., 2018. Anal. Chem. 90, 13723–13728.
Jiang, Y., Li, B.L., Milligan, J.N., Bhadra, S., Ellington, A.D., 2013. J. Am. Chem. Soc. 135, 7430–7433.
Khonsari, Y.N., Sun, S.G., 2017. Chem. Commun. 53, 9042–9054.
Kitte, S.A., Gao, W.Y., Zholudov, Y.T., Qi, L.M., Nsabimana, A., Liu, Z.Y., Xu, G.B., 2017. Anal. Chem. 89, 9864–9869.
Lee, O.P., Yiu, A.T., Beaujuge, P.M., Woo, C.H., Holcombe, T.W., Millstone, J.E., Douglas, J.D., Chen, M.S., Fréchet, J.M.J., 2011. Adv. Mater. 23, 5359–5363.
Li, D.D., Cheng, W., Li, Y.J., Xu, Y.J., Li, X.M., Yin, Y.B., Ju, H.X., Ding, S.J., 2016. Anal. Chem. 88, 7500–7506.
Li, L.Q., Li, X.L., Wang, L., Du, W.J., Guo, R., Liang, H.H., Liu, X., Liang, D.S., Lu, Y.J., Shan, H.L., Jiang, H.C., 2012. Cell. Physiol. Biochem. 30, 631–641.
Liu, S.F., Fang, L., Wang, Y.Q., Wang, L., 2017a. Anal. Chem. 89, 3108–3115.
Liu, Y.T., Wang, H.J., Xiong, C.Y., Chai, Y.Q., Yuan, R., 2017b. Bionsens. Bioelectron. 87, 779–785.
Miao, W., 2008. Chem. Rev. 108, 2506–2553.
Shen, W., Yu, Y.Q., Shu, J.N., Cui, H., 2012. Chem. Commun. 48, 2894–2896.
Si, M.L., Zhu, S., Wu, H., Lu, Z., Wu, F., Mo, F.F., 2007. Oncogene 26, 2799–2803.
Tang, Y., Zhang, X.L., Tang, L.J., Yu, R.Q., Jiang, J.H., 2017. Anal. Chem. 89, 3445–3451.
Tian, L., Qian, K., Qi, J.X., Yao, C., Song, W., Wang, Y.H., 2018. Bionsens. Bioelectron. 99, 564–570.
Wang, J.X., Zhuo, Y., Zhou, Y., Wang, H.J., Yuan, R., Chai, Y.Q., 2016a. ACS Appl. Mater. Interfaces 8, 12968–12975.
Wang, S.Q., Yang, F., Jin, D., Dai, Q., Tu, J.Y., Liu, Y.J., Ning, Y., Zhang, G.J., 2017. Anal. Chem. 89, 5349–5356.
Wang, Y.Z., Hao, N., Feng, Q.M., Shi, H.W., Xu, J.J., Chen, H.Y., 2016b. Bionsens. Bioelectron. 77, 76–82.
Wu, L., Ding, F., Yin, W.M., Ma, J., Wang, B.R., Nie, A.X., Han, H.Y., 2017. Anal. Chem. 89, 7578–7585.
Xu, A.G., Chao, L., Xiao, H.B., Sui, Y.Y., Liu, J., Xie, Q.J., Yao, S.Z., 2018. Bionsens. Bioelectron. 104, 95–101.
Xu, J.J., Huang, P.Y., Qin, Y., Jiang, D.C., Chen, H.Y., 2016. Anal. Chem. 88, 4609–4612.
Xue, T., Jiang, S., Qu, Y.Q., Su, Q., Cheng, R., Dubin, S., Chiu, C.Y., Kaner, R., Huang, Y., Duan, X.F., 2012. Angew. Chem. Int. Ed. 16, 3822–3825.
Yin, F.F., Liu, H.Q., Li, Q., Gao, X., Yin, Y.M., Lin, D.B., 2016. Anal. Chem. 88, 4600–4604.
Ye, S.J., Li, X.X., Wang, M.L., Tang, B., 2017. Anal. Chem. 89, 5124–5130.
Yin, H.S., Li, B.C., Zhou, Y.L., Wang, H.Y., Wang, M.H., Ai, S.Y., 2017. Bionsens. Bioelectron. 96, 106–112.
Zhang, J.P., Li, C., Zhi, X., Ramon, G.A., Liu, Y.L., Zhang, C.L., Pan, F., Cui, D.X., 2016. Anal. Chem. 88, 1294–1302.
Zhang, P., Wu, X.Y., Yuan, R., Chai, Y.Q., 2015. Anal. Chem. 87, 3202–3207.
Zhang, Y., Yang, H.M., Cui, K., Zhang, L.N., Xu, J.M., Liu, H., Yu, J.H., 2018. J. Mater. Chem. A 6, 19611–19620.
Zhao, H.F., Liang, R.P., Wang, J.W., Qiu, J.D., 2015. Chem. Commun. 51, 12669–12672.
Zhao, X.C., Zhou, W.J., Lu, C., 2017. Anal. Chem. 89, 10078–10084.
Zhou, B., Zhu, M.Y., Hao, Y., Yang, P.H., 2017. ACS Appl. Mater. Interfaces 9, 30536–30542.